Int J CARS
DOI 10.1007/s11548-015-1244-8

ORIGINAL ARTICLE

Robot guidance of an ultrasound probe toward a 3D region of interest detected through X-ray mammography

Marie-Aude Vitrani[1,2,3] · **Anja Marx**[1,2,3,4] · **Răzvan Iordache**[4] · **Serge Muller**[4] · **Guillaume Morel**[1,2,3]

Received: 26 March 2015 / Accepted: 5 June 2015

Abstract
Purpose This research is situated in the context of breast cancer detection where the standard procedure is the succession of an initial mammography (MX) examination and a supplementary ultrasound (US) scan. One major difficulty of this procedure results from the fact that breast geometry changes between both examinations due to different patient's positions. The proposed system facilitates this combined examination by keeping the breast geometry and by adding a US probe guidance robot to the mammography system.
Methods A comanipulation system is set up where the robot and user simultaneously manipulate the probe toward the target previously localized in MX images. Calibration procedures and robot control are detailed.
Results A test protocol was presented to conduct two tests that are both related to the medical application. The first tests aim at evaluating robot guidance for localizing a lesion which was previously defined in the X-ray images. The second tests aim at quantifying robot influence when scanning a target lesion. The studied task consists of a pointing/scanning exercise, where the US beam intersects a breast lesion.
Conclusions The experiments show a significant increase in examination quality when using robot guidance as compared to the nonassisted examination.

Keywords Comanipulation · Human–robot collaboration · Breast cancer detection · Assisted gesture

Introduction

This work is set in the medical context of breast cancer (BC) detection. The usual BC detection procedure schedules a first X-ray examination [called mammography (MX), Fig. 1] followed by a supplementary MX plus Ultrasound (US) examination if necessary, Fig. 2.

MX and US are both used because they represent complementary modalities in breast imaging. MX has proven to be very effective detecting early cancers in mostly adipose breasts, while US is more sensitive in dense breasts. For dense breasts, tissue characteristics sometimes prohibit accurate BC identification. As a result, about half of cancers with histological confirmation were missed using MX during a study on patients with dense breasts [1]. Meanwhile, attempting BC detection in women having dense breasts remains essential as 50 % appx. of young women have such breasts [9]. Furthermore, BC risk increases by a factor of 4–6 for women having dense breasts [12]. US is thus used in combination with MX as it has been reported, to be more sensitive than MX for BC detection in dense breasts, [5,11,13,15,17]. Therefore, combining MX and US into a single examination has the potential to provide an effective tool for BC diagnosis in women with dense breasts.

One of the main problems in conducting MX followed by manual US is the change of breast geometry. Indeed, in MX, the breast is compressed between the image receptor

✉ Marie-Aude Vitrani
marie-aude.vitrani@upmc.fr; vitrani@isir.upmc.fr

Anja Marx
marx@isir.upmc.fr

Guillaume Morel
morel@isir.upmc.fr

[1] UMR 7222, ISIR, Sorbonne Universités, UPMC Univ. Paris 06, Paris, France

[2] INSERM, U1150, Agathe-ISIR, 75005 Paris, France

[3] CNRS, UMR 7222, ISIR, 75005 Paris, France

[4] GE Healthcare, Buc, France

Fig. 1 MX examination

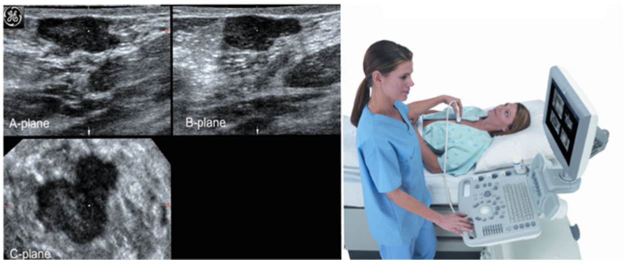

Fig. 2 US examination

and a compression paddle before X-ray exposure. On the other hand, for US, the patient is lying on her back and the breasts are not compressed anymore. The examiner has to mentally correlate the suspicious zone identified in the MX images with the new geometry of the uncompressed breasts. Conway et al. [6] reported in their study that examiners fail to locate up to 10 % of the lesions during manual US: In 10 % of manual US following MX, the examiner was going to investigate a different breast lesion than the one previously seen in MX and was not aware of the mismatch.

To overcome these difficulties, Kapur et al. [14] proposed an imaging apparatus to combine MX and automated US scans (see Fig. 3). Two degrees of freedom (DOFs) robotized probe holding framework are mounted on top of the compression paddle. During the US examination, the probe is automatically moved over the compression paddle and the images are further treated in order to display the scanned US volume. MX and US images are displayed in real time. Since US coupling gel might have a negative effect on MX image quality, MX is performed prior to US. A clear advantage of this approach is that the patient's breast remains under the same compression during MX and US. A drawback in the context of diagnostic procedures is that it may take time to fully scan the breast volume with the US probe, while the medical need is often to check a particular suspicious region that was detected on MX. Moreover, when shadows appear from either anatomical structures or paddle support, it is not possible to adapt the probe's orientation because of the limited DOFs of the scanning device.

The concept developed in this paper uses the same idea of performing the US examination right after the MX imaging, the patient's breast remaining under the same compression. However, instead of an automatic scanning with limited number of DOFs, we propose a manual manipulation of the US probe toward a target localized in the MX image, with six DOFs. This manipulation is assisted by a comanipulated system.

Comanipulation consists in sharing the control of a tool between a user and a robot. A typical behavior is set through *virtual fixtures*. Virtual fixtures are geometrical constraints imposed by a robot to a tool: Along some DOFs, the movement is free for the user while along the others, it is blocked up to the robot programmable stiffness.

This idea was implemented in [19,20], through a semi-passive device called passive arm with dynamic constraints (PADyC). Its mechanical design enables the motion of a tool to be limited in accordance with a planned task. A geometric zone is defined in which the surgeon can move freely. When moving out of the zone the surgeon is restricted by forces applied by the robot, which prevents the tool from leaving the prescribed zone. Since then, comanipulation and virtual fixtures have been widely used for surgical applications ranging from orthopedic surgery, [3,7,10] to eye surgery [16], through keyhole interventions, [18]. The application of comanipulation to the placement of an US probe following an MX exam for BC detection is detailed in "Proposed approach" section. This application requires a full system

Fig. 3 Semi-automated US breast scanning system [14]

calibration, which is described in “System calibration” section and an original controller described in “Robot control” section. A set of in vitro experimental results is given and discussed in “Experiments” section prior to a conclusion (“Discussion and conclusions” section).

Proposed approach

The workflow of the proposed system begins with a 3D mammography so-called digital breast tomosynthesis (DBT) scan of the patient’s breast (see Fig. 4). After 3D reconstruction of the breast, a suspicious zone is identified. Its coordinates are sent to the robot in order to provide assistance when locating the target lesion. The user jointly manipulates the probe with the robot. His/her task is to image the suspicious zone while maintaining contact between the probe and the paddle. The robot task is to help the radiologist, thanks to virtual fixtures (see Fig. 4). Indeed, from the physician’s point of view, the US scan remains complex: To position the probe, the shape and 3D location of the suspicious lesion must still be mentally reconstructed from the DBT images. This computation can be performed easily by a computer, and the information can then be sent to a robot, which should guide the physician toward the lesion with increased speed and accuracy. Figure 5 depicts the complete setup built to experiment this idea. A Virtuose 6D (Haption, France) robot is used. It is a fully actuated 6-DOF haptic robot which is designed to produce forces and moments at its end-effector with a high fidelity. Adaptable fixations were built to mount on the robot end-effector, a 9L linear transducer (Ultrasonix, France) connected to an Ultrasonix RP Ultrasound system.

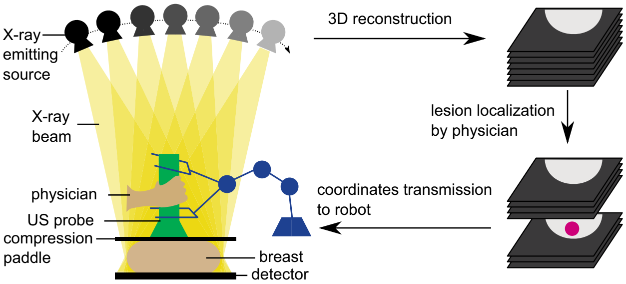

Fig. 4 Novel system for robot assistance for combining US and DBT examinations

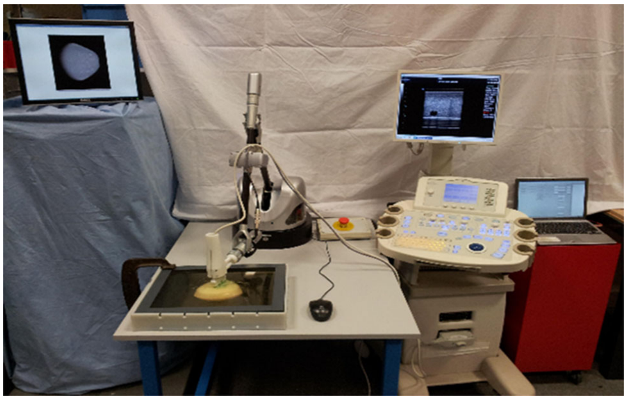

Fig. 5 Test setup

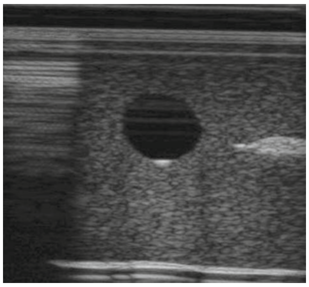

Fig. 6 US image during tests. *Left* breast border, *Top* artifacts due to compression paddle, *Bottom* artifacts due to plate simulating the detector, *Middle* cystic lesion (*black*) and tumor lesion (*white*)

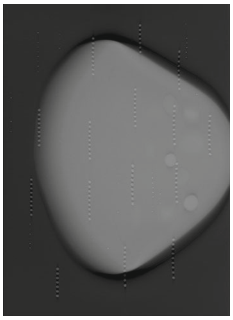

Fig. 7 X-ray image during tests

As for the breast, a multimodal breast phantom (Cirs inc. model 051 phantom) containing dense masses of 2–8 mm diameter and cystic lesions of 3–10 mm diameter is used. It is compressed between a 25-mm-thick PVC plate (at the bottom) and a 6-mm-thick PMP plate (at the top), both well suited regarding their low X-ray attenuation, PMP being equally well suited to let pass US [4]. Figure 6 shows typical US image of a lesion obtained with this setup. A computer screen is placed in front of the subject and displays the reconstructed slices of the breast phantom, acquired using an investigational DBT device based on a Senographe DS (GE Healthcare, Chalfont St Giles, UK). The subjects are free to navigate within the DBT images using the scroll ball of a computer mouse, as it is done during the standard workflow of mammography image reading (Fig. 7).

System calibration

The proposed approach leads to calibration and registration issues. The target I is first identified in the MX images. Its position in the breast phantom is thus known w.r.t. the

X-ray DBT reconstructed slices. The aim is to program the robot assisting the positioning of the probe toward the target. Therefore, it is required to determine the position of I w.r.t. the ultrasound probe. Two pieces of information are necessary:

- the US beam localization in robot base (Fig. 8), expressed through the homogeneous translation matrix M_{0P}, resulting from the product of:
    - the robot end-effector localization w.r.t. the robot base, M_{06}, (calibration detailed in “Robot identification” section),
    - and the US beam localization w.r.t. the robot end-effector, M_{6P}, (calibration detailed in “Ultrasound probe to robot end-effector localization” section),
- the X-ray image frame localization w.r.t. the robot base, M_{0X}, (Fig. 9) (registration detailed in “X-ray image registration” section).

In the next, the following coordinate frames will be used:

- $\mathscr{F}_P = (P, \mathbf{x}_P, \mathbf{y}_P, \mathbf{z}_P)$, the frame attached to US probe, with P being the probe tip and $\mathbf{z}_P$ the normal vector of the US plane. Note that $(P, \mathbf{x}_P, \mathbf{y}_P)$ is the US image plane.
- $\mathscr{F}_0 = (O_0, \mathbf{x}_0, \mathbf{y}_0, \mathbf{z}_0)$, the frame attached to the robot base.
- $\mathscr{F}_6 = \{O_6, \mathbf{x}_6, \mathbf{y}_6, \mathbf{z}_6\}$ the coordinate system of the robot end-effector.
- $\mathscr{F}_X = \{O_X, \mathbf{x}_X, \mathbf{y}_X, \mathbf{z}_X\}$ the coordinate system of the X-ray DBT reconstructed slices, with O_X being the upper-left image corner and $\mathbf{z}_X$ the image’s normal vector.

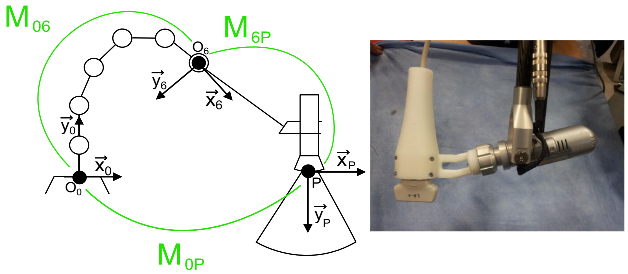

Fig. 8 Ultrasound probe to robot base calibration principle

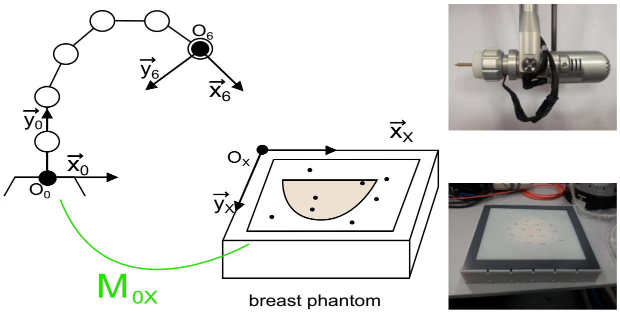

Fig. 9 X-ray image to robot base registration principle

Robot identification

In this system, a cable-driven robot is used. This type of robot may show internal position errors due to their mechanical structure (cable deformations). To interpret the calibration and registration results in their given context, the precision of the robot was determined first. A conventional geometry calibration procedure was run, leading to the identification of the Denavit–Hartenberg (DH) parameters for the Virtuose 6D [8]. DH parameters correspond to the geometrical constants of the robot (link lengths, angles between axes).

The identification consists in minimizing (with an iterative least-squares algorithm) the error between two measures of the position of a given end-effector point M. The first measure is obtained from the robot joint sensors and a geometrical model involving the DH parameters to be identified. The second measure is obtained from an external reference measure. In these experiments, the Polaris visual tracking system (Northern Digital Inc.) with a known position error noise of 0.4 mm was used for reference measures, while a visual marker was fixed at the robot end-effector (point M). The robot was positioned in different configurations, and the robot and marker positions are recorded in both systems, respectively (i.e., Virtuose 6D and Polaris) (see Fig. 10). A total of 37 measures have been used for the identification. The mean end-effector position error after convergence was 1.64 mm (max 2.65 mm, SD 0.64 mm). The optimized parameters were verified with 13 points not used for optimization, giving an average error of 1.49 mm (max 2.64 mm, SD 0.81 mm).

Ultrasound probe to robot end-effector localization

Calibrating the US probe with respect to the robot end-effector aims at localizing every US image pixel in the robot end-effector frame, i.e., determining the transformation matrix M_{6P} between $\mathscr{F}_6$ and $\mathscr{F}_P$. The approach depicted in [21] is used: A rectilinear rod plunged in a water tank is

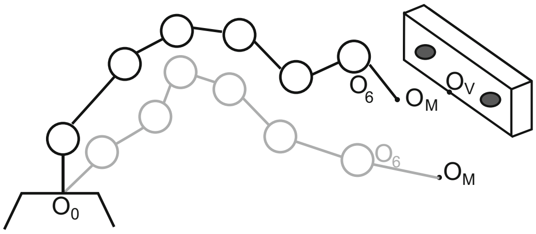

Fig. 10 Verification results of the DH identification algorithm for the Virtuose 6D robot

observed by the US probe for several robot configurations (see Fig. 11). The intersection of the calibration rod with the US plane results in a white blob in a mostly black US image, and thus, its geometrical center (GC) can easily be localized in the US image. The identification procedure consists in minimizing (thanks to a recursive least-squares algorithm) the error between two different measures of the GC coordinates in the end-effector frame. One results from the geometrical model of the robot and the other from image processing. Note that the identification procedure also allows for identifying the US image gains, namely the mm to pixel ratio (see [21]). The calibration algorithm is ran from 16 configurations. It converges with an average error of 1.17 mm (max 2.41 mm, SD 0.60 mm). In the US image, these correspond to a reconstructed error per direction of 3.12 pixels (max 8.42 pixels) and 7.66 pixels (max 18.22 pixels) in x-direction and y-direction, respectively. The optimized parameters were verified with 7 points not used for optimization. Verification terminated with an average error of 0.78 mm (max 1.74 mm, SD 0.51 mm) (see Fig. 12). In the image, these correspond to a reconstructed error per direction of 1.42 pixels (max 3.60 pixels) and 5.77 pixels (max 12.86 pixels) in x-direction and y-direction, respectively.

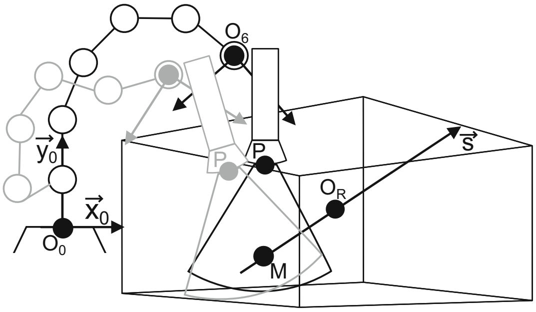

Fig. 11 Geometrical model For US probe calibration

X-ray image registration

Since the robot is not localized with respect to the mammography device, a registration step is necessary to obtain the transformation matrix between $\mathscr{F}_0$ and $\mathscr{F}_X$. The chosen method relies on measuring the coordinates of reference points in both the robot and X-ray image space. The registration tool is a nylon plate containing 15 lead ball bearings (BBs), which was positioned on top of the breast phantom. Fiducial markers have been randomly placed on a plate covering the entire breast phantom surface. The markers are 1-mm-diameter BBs highly visible in X-ray images. An X-ray scan of the registration plate is performed. The BB coordinates are determined in the X-ray images. To obtain the coordinates of the target points in the robot space, a localization tip was used. Each target point coordinates w.r.t. the robot base are computed, thanks to DH parameters identified in "Robot identification" section and to a tool model.

The registration points on the nylon paddle are determined in the robot base by manually pointing on them using the robot equipped with the calibrated tool (see Fig. 13). During this phase, the robot is controlled to apply a null force and it can be easily moved, thanks to its high backdrivability. The obtained coordinates are then mapped to the point coordinates determined in the MX images. This mapping is done using an iterative closest point algorithm (ICP) [2].

Nine marker coordinates are used to optimize the transformation parameters. The remaining five points are used to verify the optimization algorithms and to confirm the error. The chosen target points for optimization and validation are

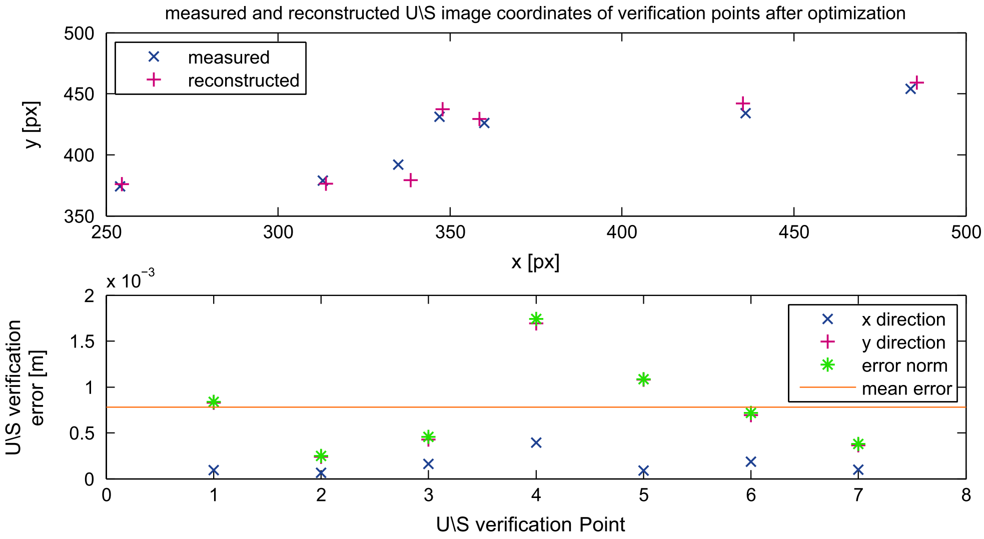

Fig. 12 Parameter verification for ultrasound probe calibration

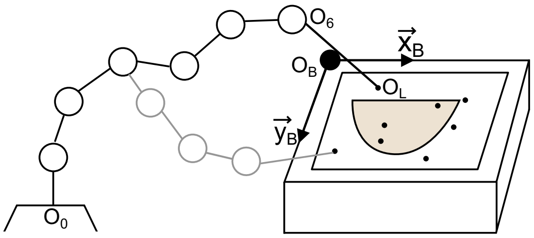

Fig. 13 Geometrical model for X-ray image registration

distributed all over the registration plate. The ICP algorithm terminates with an average error of 0.70 mm (max 1.06 mm, SD 0.24 mm). The optimized parameters were verified with 5 points, giving an average error of 0.73 mm (max 1.59 mm, std 0.48 mm) (see Fig. 14).

Total setup error

To estimate the final setup error, six target points (lesion GC of the anatomic phantom) were chosen. Their coordinates were determined in the X-ray and US images. For the latter ones, the US probe was positioned manually. After successful calibration of each system component, both independent ways to measure the same target point should give the same result. A difference between both measures indicates a calibration/registration error of the system. Thus, the GC was measured in $\mathscr{F}_P$ and $\mathscr{F}_X$ separately. To estimate the error between both sets, they were expressed in $\mathscr{F}_P$. The transformation from $\mathscr{F}_X$ to $\mathscr{F}_P$ is possible, thanks to the previous calibration steps. Indeed, any point $Q_X|_X$ expressed in $\mathscr{F}_X$ can be expressed in $\mathscr{F}_P$ by:

$$Q_X|_P = M_{PX} Q_X|_X = M_{P6}\, M_{60}\, M_{0X}\, Q_X|_X \tag{1}$$

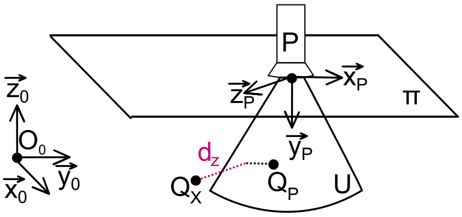

Fig. 15 Geometrical model total setup error

Target points have been identified in the breast phantom to estimate the total setup error. The point coordinates have been determined in the X-ray images (Q_X in Fig. 15). The same target points have been visualized using US and are denoted Q_P. Thanks to the previous probe to end-effector calibration, the distance between Q_X and the US beam could be calculated:

$$d_z = \left|(Q_X - Q_P)^{\mathrm{T}} \mathbf{z}_P\right| \tag{2}$$

The average distance between the GC measured in X-ray images and the US beam is 1.29 mm (max 2.23 mm, std 0.84 mm) (see Fig. 16). Note that this estimation depends on the manual position capabilities. A human error is thus induced in this procedure. Nevertheless, the US probe was positioned by a user who already knew the breast phantom while paying much attention. The total setup error is due to the following identified possible sources of error:

- the robot internal position error,
- the BBs used for registration and their diameter of 1 mm,
- the reconstruction distance of 0.5 mm between the X-ray image slices (relatively low resolution),
- the localization-tip diameter of 0.25 mm,

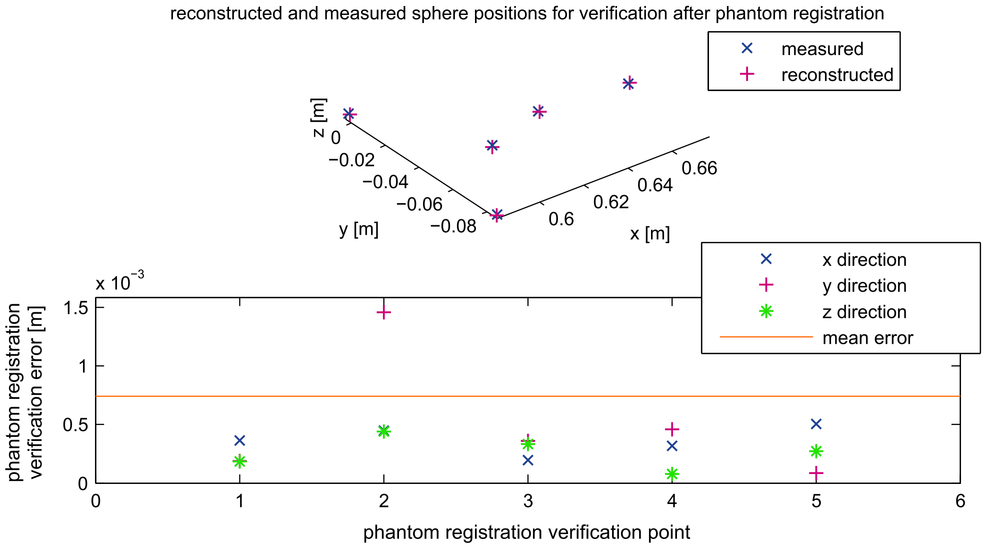

Fig. 14 X-ray image to robot verification

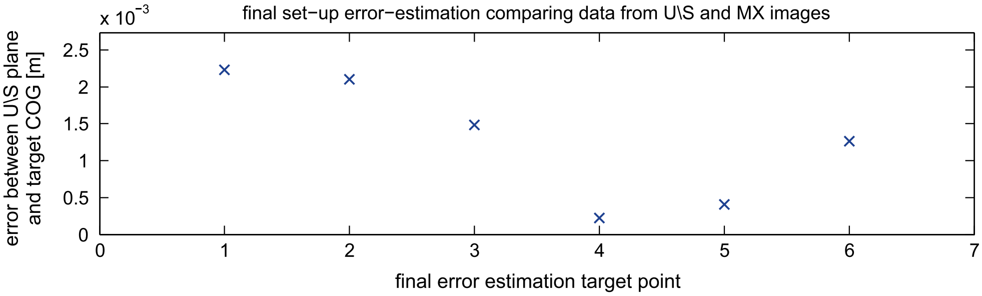

Fig. 16 Total setup error

Taking into account the medical context in which this system would be used, the total error looks pretty acceptable. Indeed, the smallest lesions detected in clinical practice with US are about 5 mm in diameter.

Robot control

Robot-assisted US examination of BC detection can be modeled as a pointing/scanning task where the user is assisted by a robot, who knows the location of the lesion. Since the breast remains compressed after MX, the US scan is to be performed through the compression paddle. The radiologist's task is to find and scan the suspicious zone while maintaining contact between the probe and the paddle. For better visibility, physicians often display the lesion in the middle of the US image, on its main axis. The task of a conventional US scan has a total of six DOFs. However, it can be reduced to a four-DOF task at the probe tip, thanks to the assumption of constant probe–paddle contact. Two movements would lead to a loss of probe–paddle contact and thus are not part of the task:

- translations along the paddle normal vector,
- rotations around vector normal to the US beam.

The positioning task possesses thus four DOFs, as shown in Fig. 17: two translations of the probe tip on the paddle, assumed to be planar, one rotation along the normal vector of the paddle surface, and a second rotation around the intersection line of the paddle surface and the US plane. Even if the task is associated with scanning, i.e., the full coverage of a region of interest (ROI), this can be reduced to a pointing task based on the hypothesis of a moving point of interest (POI) within the ROI. The compression paddle is associated with a plane π, while the ultrasound beam plane is denoted U. In the next, the following notations are used:

- The US probe is handled by the user at point H on the US probe main axis.
- The robot wrench is applied on the probe at point R on the US probe main axis.
- The central point of the suspicious lesion S is denoted I and its projection on U is denoted I_1 with $I_1 - I = l_1 \mathbf{z}_P$.
- The projection of I on the US probe main axis is denoted I_2, $I_2 - I_1 = l_2 \mathbf{x}_P$.

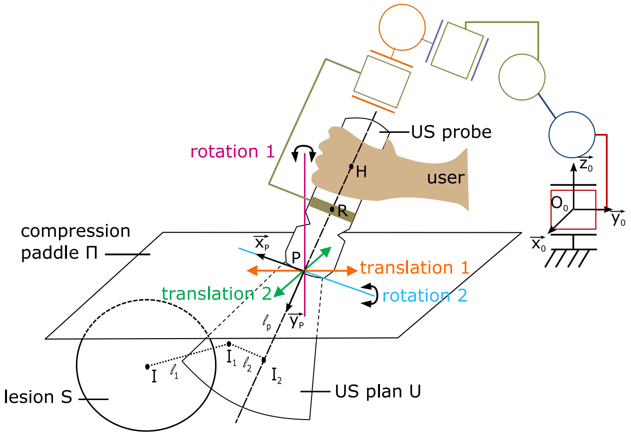

Fig. 17 DOF of a US scan of a compressed breast through a rigid compression paddle

The task consists of centering the suspicious lesion in the image, which is hence divided into two parts:

1. assuring intersection between the US plane and the lesion ($I = I_1$),
2. centering the lesion in the image ($I_1 = I_2$).

As stated in "Introduction" section, it is important to allow imaging tissues surrounding the lesion, as well as letting the radiologist to choose the probe orientation in order to avoid undesired shadows and to observe the lesion from a desired angle of view. Consequently, the robot should not completely prevent the user from moving away from the target. To simulate such behavior, a robot control that generates a wrench corresponding to the sum of two compression springs of stiffness, k_1 and k_2, respectively, was implemented. Both springs have a null-free length. One connects I and I_1, whereas the second one connects I_1 and I_2:

$$\mathscr{E}_1 = \left[0\ 0\ -k_1 l_1\ 0\ 0\ 0\right]^{\mathrm{T}}_{I_1}; \quad \mathscr{E}_2 = \left[-k_2 l_2\ 0\ 0\ 0\ 0\ 0\right]^{\mathrm{T}}_{I_2} \quad (3)$$

The applied wrenches thus provide a state of equilibrium at $I = I_1$ and $I_1 = I_2$, when the task is successfully accomplished. The complete wrench applied to execute the task is the sum of $\mathscr{E}_1$ and $\mathscr{E}_2$:

$$\begin{aligned}\mathscr{E}_{\text{task}} &= \mathscr{E}_1 + \mathscr{E}_2 & (4)\\ &= \left[-k_2 l_2\ 0\ -k_1 l_1\ -k_1 l_1 l_P\ \ -k_1 l_1 l_2\ \ k_2 l_2 l_P\right]^{\mathrm{T}}_P & \\ &\quad \text{with } (I_2 - P) = l_P \mathbf{y}_P. & (5)\end{aligned}$$

This controller is applied to the robot at a 1 kHz rate. In order to ease the manipulation, a viscosity term depending on the end-effector velocity at O_6 is added for proper damping, while a gravity compensation of the US probe's weight is added.

Experiments

Protocol

Tests have been performed by 22 naive subjects using the setup. A large number of subjects have been recruited to account for inter-subject variability and still obtain statistically significant results. It was not possible to recruit such a large number of radiologists. This is why the results are not to be considered as an absolute performance evaluation but, rather, as a differential comparison between assisted and nonassisted manipulation. Notice that since the task to be realized is not a conventional clinical gesture, even radiologists would have been considered as naive subjects with respect to the task and the robot assistance.

For Test 1, the subjects are presented with a target lesion chosen in the MX images. They start (at $t = 0$) with the US probe in its rest position (at one corner of the breast phantom) and have to localize this particular target on the phantom using US. When subjects think they have localized the lesion from a first guess, they give a vocal feedback (at $t = t_1$). Then, they proceed to analyze the surrounding tissues (seeking for other points of interest) in order to verify their first guess, as a radiologist would do in a real situation. Once they are certain to have localized the lesion, a second vocal feedback is given (at $t = t_2$) and the test is stopped. During Test 2, the subjects are asked to scan the entire target lesion (not only its central point) using US. This corresponds to a clinical phase where the radiologist wants to characterize the lesion (shape and size). Test 2 starts (at $t = t_3$) with the US probe already positioned above the lesion to be examined. Four different scanning methods are used within Test 2. First, the user is asked to visualize the lesion in the US images under as many different perspectives (probe orientations) as possible within 30 s. For the three remaining scanning methods, the subject is asked to execute a particular movement and has only 10 s to scan the lesion. Three movements compatible with the probe–paddle contact geometry are selected: translations along the compression paddle plane, rotations around the paddle normal vector $\mathbf{n}_\pi$ and rotations around the intersection of the US plane and the paddle surface ($\mathbf{z}_P \times \mathbf{n}_\pi$). Test 2 terminates at $t = t_e$. The two tests performed are summarized here (see Fig. 18):

- Test 1: subtasks one and two: approximate target localization followed by proper target identification.
- Test 2: subtask three: entire target lesion scan.

The test are run under two conditions: Either the robot is in a transparent mode (no forces applied, mode 1), or the robot applies the elastic force fields depicted in "Robot control" section (mode 2). To avoid increasing learning effects, all Tests 1 (for both actuation modes) have been executed in a row and prior to Tests 2. The subjects have thus not been habituated to the phantom geometry during Tests 1. User performances for each mode were compared. For Tests 1, two performance indicators were chosen:

- US plane-to-target distance (precision), $d_z = \text{mean}\left(\left|(I - I_1)^{\mathrm{T}} \mathbf{z}_P\right|\right)$,
- completion time (duration), t_2.

In order to compare the different time performances, they were normalized over the entire duration of the series of Tests 1 for each subject and both actuation modes, e.g., for mode i: $t_{l,i} = \dfrac{t_{2,i} - t_{0,i}}{\sum_1^2 (t_{2,i} - t_{0,i})}$.

Results of Tests 2 have been grouped for each actuation mode, independent of the movement. The performance indicators are:

- The visibility ratio t_{s} defined as the ratio between the time span when US plane U and lesion volume S intersect (i.e., when the lesion is visible) and the total duration of the scanning test: $t_{\mathrm{s}} = \frac{t'_{\mathrm{s}}}{t_e - t_2}$, with $t'_{\mathrm{s}} = \sum_{t_2}^{t_e} (t_i - t_{i-1}), \forall t_i \in$

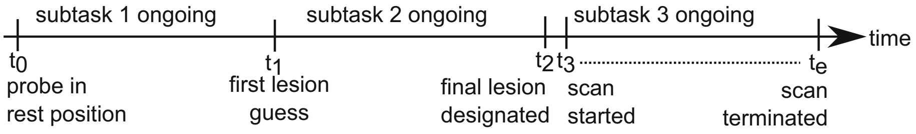

Fig. 18 Time line for Tests

$\{t_3, \ldots, t_e\} : (S \cup U)$ and $t_e - t_2 = 30$ s as imposed by the protocol.

- the US plane-to-target distances (precision), $d_z = \text{mean}\left(|(I - I_1)^{\mathrm{T}} \mathbf{z}_P|\right)$,

Test data have been analyzed using statistical ANOVA (analysis of variance) tests. It indicates whether or not the results obtained per control mode are significantly different. The result of ANOVA tests gives so-called p and F values which have to be interpreted w.r.t. level of confidence as shown here:

- the F-value is the ratio of the variance *between* control modes and the variance *within* each control mode. It quantifies the separation of each sampling group (here control mode) w.r.t. the others. The higher the F value, the more the samplings (control mode) are significantly different.
- the p value depends on the actual F value. A low p value indicates a high confidence in the given statistical result. For a low p value, it is highly probable that the control modes have significant influence on user performances.

In case of $p < 0.05$, one can conclude that the robot control modes have altered the effects on user performances in relation to the analyzed data to a significance level of 95 %.

Results

Table 1 shows the number of properly located lesions for each control mode at the end of Tests 1.

Table 2 shows how subjects changed their guess between the first and second feedback. Without guidance, two subjects rectified their first guess, and one finally chose a wrong lesion as target although it was properly localized at the first feedback. One subject rectified his initial guess with assistance, in a positive way.

Indicators for Tests 1 averaged across subjects are plotted in Fig. 19. The average normalized time needed to localize the lesion was longer in mode 1 ($\bar{t}_{l,1} = 58.1\,\%, \sigma = 15.1\,\%$) than in mode 2 ($\bar{t}_{l,2} = 42.0\,\%, \sigma = 15.1\,\%$), which represents a 28.0 % time reduction brought by the robot guidance. Users also performed worst with mode 1 regarding precision. In this mode, the average US plane-to-target distance ($\bar{d}_z$) is 0.8 cm (1.43 cm), while it is only 0.05 cm (0.17 cm) in mode 2. This represents an improvement of 94.0 % brought by robot guidance. This accuracy can be considered sufficient to image lesions of 0.5 cm diameter in practice.

Table 1 Number of properly located lesions during Tests 1 over 22 subjects

Actuation mode	1 (Without guidance)	2 (With guidance)
Results at $t = t_1$	12	14
Results at $t = t_2$	13	15

Table 2 Change of chosen lesion between both feedbacks during Test 1

Actuation mode	1 (Without guidance)	2 (With guidance)
Wrong → proper	2	1
Proper → wrong	1	0
No change, wrong	8	7
No change, proper	11	14

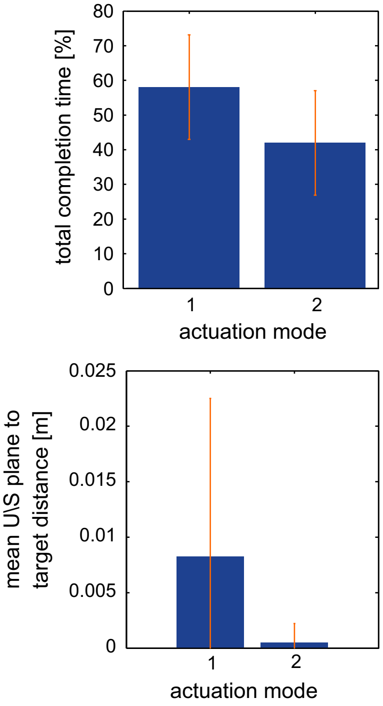

Fig. 19 Results of Tests 1: mean localization time and US plane-to-target distance

One-factor ANOVA with subjects as repeated measures was used to analyze each indicator. The robot guidance has a significant effect on the US plane-to-target distances ($F = 7.2$ and $p = 0.014$). Results of completion time ($F = 6.3$ and $p = 0.020$) showed a less but still significant effect for the experiment conditions. Indicators for Test 2 are plotted in Fig. 20. With mode 1, the visibility ratio $\bar{t}_s$ averaged across subjects was 56.7 % (SD 3.3 %) of the total duration of Tests 2. Users have thus only spent about half of the time imaging the lesion, and the rest of the time, it was not visible in the US images although they were explicitly asked to maintain visibility during the scanning movement. With mode 2, $\bar{t}_s$ reached 89.8 % (SD 3.4 %). The target-to-plane distance averaged across subjects, $\bar{d}_z$, was analyzed regarding its mean

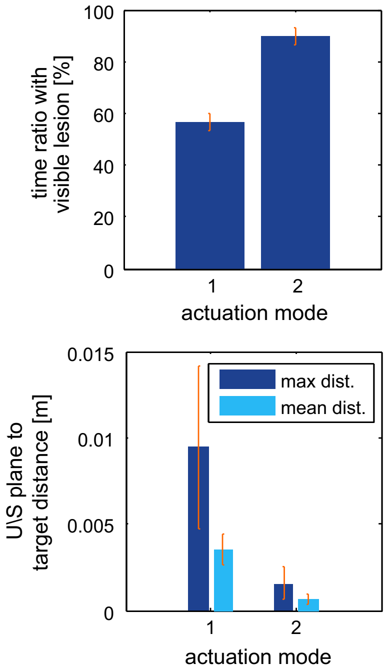

Fig. 20 Results of Tests 2: results for visibility ratio and US plane-to-target distance

and maximum values across the four different scanning methods of Tests 2, denoted mean($\bar{d}_z$) and max($\bar{d}_z$), respectively. The indicator max (mean(d_z)) is larger in mode 1 [0.95 cm (SD 0.47 cm)], to be compared to 0.16 cm (SD 0.1 cm) for mode 2. The maximal distance was thus decreased by 83 % by the use of guidance. A similar relation can be observed for mean($\bar{d}_z$). Its value is 0.35 cm (SD 0.09 cm) for mode 1 and only 0.06 cm (SD 0.03 cm) for mode 2. This corresponds to an improvement of 82 %. One-factor ANOVA run with subjects as repeated measures again showed a significant effect of the two actuation modes: $F = 210.8$, $p = 0.0007$ for visibility ratio, $F = 17.2$, $p = 0.0250$ for max US plane-to-target distance and $F = 80.2$, $p = 0.003$ for mean US plane-to-target distance. p values are equally below 0.002 for results of each independent Tests 2 series (i.e., free movement or the three imposed movements).

Discussion and conclusions

The aim of this work was to propose a solution for combining MX and US breast scans without changing the breast geometry. This is motivated by clinical literature reporting diagnostic errors due to breast geometry changes between MX and US examinations. In order to minimize the dual-examination duration, which is crucial as breast compression induces pain to the patient, we have proposed to assist the physician in locating, with the US probe, a lesion identified in the 3D MX images. A comanipulated robot was developed to help scanning the breast with an US probe through the MX compression paddle.

In order to allow for immediate operation as soon as the patient is installed, we have proposed to install the robot fixed w.r.t. the DBT imaging device and to calibrate the system. The overall system precision is 1.29 mm, which is sufficient with regard to the clinical application, where lesions of 5 mm need to be identified.

A test protocol was presented to conduct two tests that are both related to the medical application. The first tests aims at evaluating robot guidance for localizing a lesion which was previously defined in the X-ray images. The second tests aims at quantifying robot influence when scanning a target lesion. The studied task consists of a pointing/scanning exercise, where the US beam intersects a breast lesion.

Table 1 shows a slight increase in the ability of properly identifying the target lesion thanks to the use of the robot. The low stiffness used throughout the experiments in order to let the user scan the system is certainly a reason for that low improvement, which is yet of approx. 10 %. More importantly, the use of a robot increases precision during both tests, nearly 94 %. Furthermore, it decreases the time needed to properly localize a target using US by nearly 30 %. During the scanning phase, the visibility ratio was increased by 60 %, indicating that keeping the lesion visible during the US scanning phase is easier. We hypothesize that this could allow for localizing smaller lesions.

In summary, it was shown that user performance increased significantly with robot assistance in terms of speed and precision.

Acknowledgments This work is partially funded by ANRT under CIFRE Grant 247/2009 and by French state funds managed by the ANR within the Investissements d'Avenir program (Labex CAMI) under reference ANR-11-LABX-0004.

Compliance with ethical standards

Conflicts of interest The authors declare that they have no conflict of interest.

Research involving human participants All procedures performed in studies involving human participants were in accordance with the ethical standards of the institutional and/or national research committee and with the 1964 Helsinki declaration and its later amendments or comparable ethical standards. This article does not contain any studies with animals performed by any of the authors.

Informed consent was obtained from all individual participants included in the study.

References

1. Berg WA, Blume JD, Cormack JB, Mendelson EB, Lehrer D, Bhm-Vlez M, Pisano ED, Jong RA, Evans WP, Morton MJ, Mahoney MC, Hovanessian Larsen L, Barr RG, Farria DM, Marques HS, Boparai K (2008) Combined screening with ultrasound and mam-

mography vs mammography alone in women at elevated risk of breast cancer. J Am Med Assoc (JAMA) 299(18):2151–2163

2. Besl PJ, McKay HD (1992) A method for registration of 3-d shapes. IEEE Trans Pattern Anal Mach 14:227–241
3. Bonneau E, Taha F, Gravez P, Lamy S (2004) Surgicobot: surgical gesture assistance cobot for maxillo-facial interventions. Perspect Image-Guided Surg 1:353–360
4. Booi RC, Kruecher JF, Goodsitt MM, O'Donnell M, Kapur A, LeCarpentier GL, Roubidoux MA, Fowlkes JB, Carson PL (2007) Evaluating thin compression paddles for mammographically compatible ultrasound. Ultrasound Med Biol 33(3):472–482
5. Buchberger W, Niehoff A, Obrist P, DeKoekkoek-Doll P, Duenser M (2000) Clinically and mammographically occult breast lesions: detection and classification with high-resolution sonography. Semin Ultrasound CT MRI 21(4):325–336
6. Conway W, Hayes C, Brewer W (1991) Occult breast masses: use of a mammographic localizing grid for us evaluation. Radiology 181(1):143–146
7. Davies B, Fan K, Hibberd R, Jakopec M, Harris S (1997) A mechatronic based robotic system for knee surgery. In: IASTED International Conference on Intelligent Information Systems, pp. 48–52
8. Dombre E, Khalil W (2007) Robot Manipulators: Modeling, Performance Analysis and Control. Control Systems, Robotics and Manufacturing Series. Wiley-ISTE
9. D'Orsi C, Bassett L, Berg W (2003) Breast imaging reporting and data system: ACR BI-RADS-Mammography, 4th edn. American College of Radiology, Reston
10. Francoise V, Sahbani A, Morel G (2011) A comanipulation device for orthopedic surgery that generates geometrical constraints with real-time registration on moving bones. In: Robotics and Biomimetics (ROBIO), 2011 IEEE International Conference on, pp. 38–43
11. Gordon P, Goldenberg S (1995) Malignant breast masses detected only by ultrasound: a retrospective review. Cancer 76(4):626–630
12. Harvey JA, Bovbjerg VE (2004) Quantitative assessment of mammographic breast density: relationship with breast cancer risk1. Radiology 230(1):29–41
13. Kaplan S (2001) Clinical utility of bilateral whole breast us in the evaluation of women with dense breast tissue. Radiology 221(3):641–649
14. Kapur A, Carson P, Eberhard J, Goodsitt M, Thomenius K, Lokhandwalla M, Buckley D, Roubidoux M, Helvie M, Booi R, LeCarpentier G, Erkamp R, Chan H, Fowlkes J, Thomas J, Landberg C (2004) Combination of digital mammography with semi-automated 3d breast ultrasound. Technol Cancer Res Treat 3(4):325–334
15. Kolb TM, Lichy J, Newhouse JH (2002) Comparison of the performance of screening mammography, physical examination, and breast us and evaluation of factors that influence them: An analysis of 27,825 patient evaluations 1. Radiology 225(1):165–175
16. Kragic D, Marayong P, Li M, Okamura AM, Hager GD (2005) Human-machine collaborative systems for microsurgical applications. Int J Robot Res 24(9):731–741
17. Leconte I, Feger C, Galant C, Berlire M, Berg B, D'Hoore W, Maldague B (2003) Mammography and subsequent whole-breast sonography of nonpalpable breast cancers: the importance of radiologic breast density. Am J Roentgenol 180(6):1675–1679
18. Poquet C, Vitrani MA, Morel G (2014) Proximal comanipulation of a minimally invasive surgery instrument to emulate distal forces. In: CRAS 2014, 4th Joint Workshop on New Technologies for Computer/Robot Assisted Surgery, pp. 48–51
19. Schneider O, Troccaz J (2001) A six degree of freedom passive arm with dynamic constraints (padyc) for cardiac surgery application: preliminary experiments. Comput Aided Surg 6:340–351 (**special issue on medical robotics**)
20. Schneider O, Troccaz J, Chavanon O, Blin D (2000) Padyc: a synergistic robot for cardiac puncturing. In: IEEE International Conference on Robotics and Automation (ICRA), pp. 2883–2888
21. Vitrani MA, Morel G (2008) Hand-eye self-calibration of an ultrasound image-based robotic system. In: IEEE/RSJ International Conference on Intelligent Robots and Systems (IROS), pp. 1179–1185